Revista Brasileira de Ciência do Solo

Division - Soil in Space and Time | Commission - Soil Genesis and Morphology

Weathering of Rhyolites and Soil Formation in an Atlantic Forest Fragment in Northeastern Brazil

Stephany Alves Brilhante[(1)], Jean Cheyson Barros dos Santos[(1)], Valdomiro Severino de Souza Júnior[(2)*], Jane Kelly Silva Araújo[(1)], Mateus Rosas Ribeiro Filho[(2)] and Marcelo Metri Corrêa[(3)]

[(1)] Universidade Federal Rural de Pernambuco, Departamento de Agronomia, Programa de Pós-Graduação em Ciências do Solo, Recife, Pernambuco, Brasil.
[(2)] Universidade Federal Rural de Pernambuco, Departamento de Agronomia, Recife, Pernambuco, Brasil.
[(3)] Universidade Federal Rural de Pernambuco, Unidade Acadêmica de Garanhuns, Garanhuns, Pernambuco, Brasil.

ABSTRACT: Weathering and pedogenesis have been studied for a wide range of rocks and climates around the world. However, the eruption of rhyolitic magmas is a rare geological event, which leads to few studies associated with the rhyolite-soil-landscape relationship. In this context, this study evaluated the influence of rhyolite weathering on the properties of soils along a slope in an Atlantic Forest environment in the state of Pernambuco, northeastern Brazil. Four weathering profiles derived from rhyolites were classified and sampled for chemical, physical, mineralogical, micromorphological, differential thermal, and thermogravimetric analyses. The chemical properties reflect the original rock rich in felsic minerals, poor in bases, and the types of clay minerals. The clay fraction of the profiles consists mainly of 1:1 phyllosilicates and oxides, indicating intermediate weathering. However, variations in the degree of structure weathering were evidenced by the presence of partially preserved fragments of the original rock in the sand fraction of the soils. The tropical humid climate of the region influenced conversion of hematite to goethite through the xanthization process, and the subsurface drainage deficiency allowed the formation of halloysite in the lowest position of the landscape. Because it is an acid rock with an aphanitic texture and porphyritic relative size of crystals, rhyolite weathering resulted in the formation of dystrophic soils, with predominance of quartz in the silt fraction. From the top to the lower third of the slope, a Haplic Cambisol, an Abruptic Lixisol, and two Haplic Lixisols were formed.

Keywords: pedogenesis, halloysite, toposequence, acid crystalline rock.

*** Corresponding author:**
E-mail: valdomiro.souzajunior@ufrpe.br

Received: December 19, 2016

Approved: April 6, 2017

How to cite: Brilhante SA, Santos JCB, Souza Júnior VS, Araújo JKS, Ribeiro Filho MR, Corrêa MM. Weathering of rhyolites and soil formation in an Atlantic Forest fragment in northeastern Brazil. Rev Bras Cienc Solo. 2017;41:e0160558.
https://doi.org/10.1590/18069657rbcs20160558

INTRODUCTION

The different routes of mineralogical alterations occurring during rhyolite weathering under a humid tropical climate result in a variety of soils that are still little known (Ghani, 1996). Rhyolite-derived soils constitute a pedodiversity that supports the existence of Atlantic Forest fragments and large agricultural properties in the domains of the "Mares de Morros" on the southern coast of Pernambuco, northeastern Brazil. In this region, the weathering-soil-geomorphology relationship plays a prominent role, given the importance of the parent material and relief for the formation and distribution of the soils in the landscape.

Rhyolites are acid igneous rocks, with aphanitic texture and relative crystal size ranging from vitrophyric to porphyritic, commonly described as the extrusive equivalent of granites (Swindale and Jackson, 1960). The mineralogical constitution of rhyolites includes quartz, feldspars, biotite, amphiboles, and pyroxenes (Heckman and Rasmussen, 2011). Rhyolite formation is a rare geological event. Isolated eruptions of rhyolites have been described in the United States, Papua New Guinea, Chile, New Zealand, and Brazil (Swindale and Jackson, 1960; Kämpf, 1995; Heckman et al., 2009; Heckman and Rasmussen, 2011).

In Brazil, areas of rhyolites have been described in the Paraná Basin, in Paraná and Rio Grande do Sul state, the Espinhaço Mountains, in Minas Gerais state, and in the volcano-sedimentary Cabo Basin, in Pernambuco state (Ghani, 1996; Assis et al., 2002; Pedron, 2007). Brazilian rhyolites give rise to a diversity of soil classes, including Neosols, Cambisols, and Argisols (Ghani, 1996). Rhyolite-derived soils in Brazil usually have high silt and clay contents, properties associated with the mostly aphanitic texture of the original lithotype and with the wide formation of secondary minerals as weathering evolved, respectively (Pedron, 2007).

The clay mineral properties of rhyolite-derived soils are variable. As weathering of this rock occurs, feldspars and ferromagnesian minerals change and may lead to the formation of 2:1 and/or 1:1 clay minerals, as well as iron oxides and oxyhydroxides (hematite and goethite) and Al hydroxide (gibbsite) through the processes of bisialitization, monosialitization, and ferralitization, respectively (Heckman and Rasmussen, 2011). The aphanitic texture, when present, makes the primary constituents of the rhyolites even more susceptible to weathering, due to the increase in the specific surface of these minerals (Pedron, 2007).

Throughout the weathering of rhyolites, various factors and pedogenetic processes are responsible for variations in the morphological, chemical, physical, and mineralogical properties of the soils, especially climate, position of the soil in the landscape, local drainage, and erosion and deposition processes (Ghani, 1996). Thus, the study of profiles derived from rhyolites along a slope, or toposequence, has great importance in elucidating the mechanisms that can cause spatial variability in the properties of these soils (Ghidin et al., 2006). The southern coast of the state of Pernambuco is a region favorable to this type of study.

The rhyolite slope studied here from a fragment of the Atlantic Forest (Lima Filho et al., 1996; Nascimento et al., 2004) allows a comparative examination as to how the topography, under humid tropical climate, affects rhyolite weathering and soil formation, with an emphasis on the silt and clay fractions. To reduce gaps in knowledge regarding soils derived from acid volcanic rocks, the aim of this study was to understand rhyolite weathering in the southern coast of Pernambuco and the formation of soils along a toposequence based on their morphological, physical, chemical, and mineralogical properties.

MATERIALS AND METHODS

Collection and preparation of samples

The site under study, in geological terms, is part of the Cabo Basin, more precisely, the Ipojuca Formation in the municipality of Sirinhaém on the southern coast of Pernambuco (Figure 1). The southern coast is an economically and environmentally important area for the state.

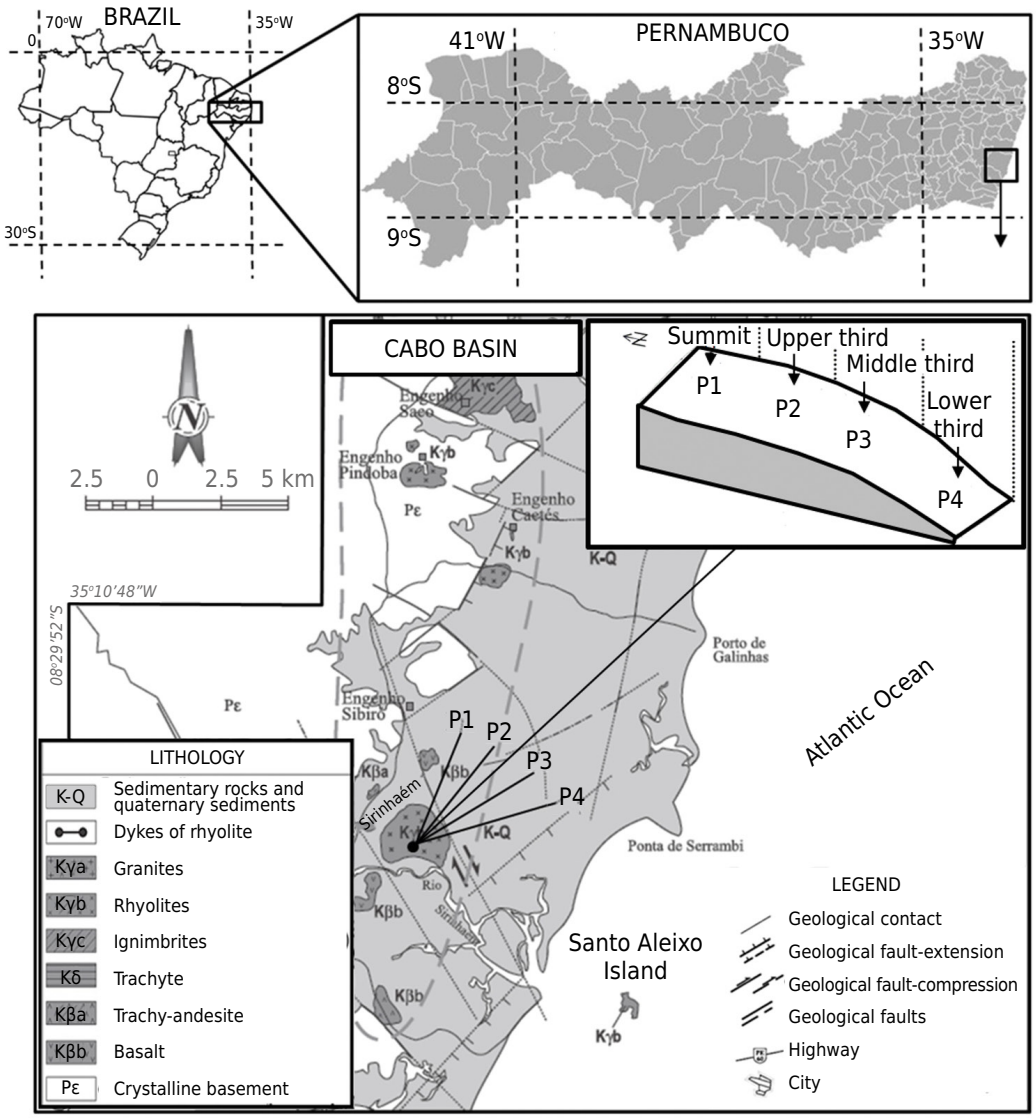

Figure 1. Location of the profiles in the volcano-sedimentary basin of Cabo (Modified from Lima Filho, 1998).

The site selected is at 08° 34' S and 35° 05' W. The soils sampled are a product of alteration of rhyolite with aphanitic texture and porphyritic relative crystal size, along with minerals larger than 2 mm, characteristic of the deepest regions of the flood basalt (Lima Filho, 1998).

The magmatic event that gave rise to the rhyolites in the Ipojuca Formation was established in the Cretaceous Period (102 Ma) during the rupture of the South American and African continents, with consequent appearance of the South Atlantic Ocean (Lima Filho, 1996; Nascimento et al., 2009). The toposequence under study is in a region with As climate, described as hot and humid, with rains in the winter (Köppen, 1931). The mean rainfall is around 2,200 mm, and the mean annual temperature is 24 °C (Silva et al., 2013).

Four soil profiles were characterized along a toposequence. Profile 1 (P1), profile 2 (P2), profile 3 (P3), and profile 4 (P4) are located on the flat top of the elevation on an undulating relief (8° 34' 3.5" S, 35° 5' 9.8" W), upper third of the elevation slope on undulating relief (8° 33' 58.5" S, 35° 8' 8.4" W), intermediate third of the convex slope on undulating relief (8° 33' 57" S, 35° 5' 8.6" W) and lower third of the convex slope on undulating relief (8° 33' 55.3" S, 35° 5' 8.8" W), with 67, 65, 53 and 36 m of altitude, respectively.

The soils were classified according to the Brazilian Soil Classification System - SiBCS (Santos et al., 2013), World Reference Base of Soil Resources (WRB, 2014), and Soil taxonomy

(Soil Survey Staff, 2014). The morphology of the soils was described in the field, and soil samples, disturbed and undisturbed, were collected in the horizons described (Santos et al., 2013). Undisturbed samples of the horizons Bi2 of P1, BC3 of P2, Bt1 and Bt3 of P3, and Bt of P4 were collected in Kubiena boxes for later impregnation and production of micromorphological thin sections. Air-dried fine earth (ADFE) was obtained after drying, fragmentation of aggregates, and sieving of the samples through a 2-mm mesh. Samples of the original rock were also collected in outcrops. The rhyolite was fragmented and reduced, and subsamples were used for mineralogical analyses.

Laboratory analyses

The following analyses were performed: ADFE particle size distribution, because of the absence of the gravel fraction. Samples from all horizons were dispersed in NaOH solution (0.1 mol L^{-1}) and sieved to separate the sand fraction through a 0.053 mm mesh. After decantation of the silt fraction, the clay fraction mass in suspension was determined based on the density of the clay-dispersant mixture corrected by the temperature, according to the method described in Gee and Or (2002). Clay dispersed in water, using a 100-g aliquot of the ADFE from each horizon subjected to dispersion in H_2O and determined by the clay-water mixture density corrected by the temperature, according to the method described in Gee and Or (2002). Soil bulk density (Bd), determined by the paraffin-clod method, as described in Blake and Hartge (1986). Particle density (Pd), determined through the volumetric flask method, as described in Flint and Flint (2002); and specific surface area (SSA) after elimination of soil organic matter with H_2O_2 (30 %), determined through the water vapor sorption method described in Quirk (1955). The results were used to estimate clay fraction activity (T), degree of flocculation (DF), silt/clay ratio, and total porosity (TP).

The chemical analyses performed were: soil pH, measured in distilled water and 1 mol L^{-1} KCl solution (1:2.5), according to the method described in Embrapa (2009); exchangeable Ca, Mg, and Al, extracted by 1 mol L^{-1} KCl and determined through atomic absorption spectrometry, based on Pansu and Gautheyrou (2006) and on the method described in Embrapa (2009); available P, determined through colorimetry, using ascorbic acid as a reducer after extraction with Mehlich-1 solution, according to the method described in Embrapa (2009); total organic carbon (TOC), through the method of Yeomans and Bremner (1988); potential acidity (H+Al), through the 0.5 mol L^{-1} calcium acetate and alkalimetric titration of the extract, according to Embrapa (2009); exchangeable Na and K, extracted with Mehlich-1 and determined through flame photometry, according to the method described in Embrapa (2009). These results were used to estimate the sum of bases (SB), cation exchange capacity (CEC), base saturation (V), and Al saturation (m).

The content of secondary iron oxides in the soil was measured using selective dissolution techniques through three successive extractions with dithionite-citrate-sodium bicarbonate (DCB) solution (Fe_d) according to Mehra and Jackson (1960) and single extraction with ammonium acid oxalate (Fe_o) according to McKeague and Day (1966). Silicon, Al, Fe, Ti, Ca, Mg, K, and P, in the form of oxides, were determined in the horizons of all profiles using an X-ray fluorescence spectrometer (XRF) (Rigaku, model RIX 3000). The results were used to calculate the Fe_o/Fe_d and $Fe_d/Fe_{t,}$ ratios, where Fe_t is the Fe determined by XRF.

One sample of unaltered rhyolite was pulverized and analyzed through X-ray diffractometry to determined its mineralogical constitution. The mineralogical constitutions of the sand, silt, and clay fractions of the upper, intermediate, and lower horizons of P1, P2, and P3 were also determined. The clay fraction was treated to remove oxides and organic matter through the addition of DCB solution and H_2O_2 solution (30 %), respectively. Treatments of saturation with $MgCl_2$ at room temperature and KCl at room temperature and 550 °C for 2 h. The samples were prepared on glass slides in the form of oriented films, to expose the plane (d_{001}) of the phyllosilicates to the diffraction, and in the form of non-oriented powder (Jackson, 1969).

Samples of the clay and silt fractions of P1 (top), P3 (representing the intermediate position), and P4 (lower third) were analyzed using a Shimadzu XRD 6000 X-ray diffractometer. Due to the low variation of mineral composition in few centimeters along the profile, diffractometry was applied only in the upper, intermediate, and lower horizons of the profiles. Scanning for samples of oriented aggregates was from 2 to 35° 2θ with a speed of 0.5° 2θ min^{-1}, operating in the continuous acquisition mode. Scanning in diffracted non-oriented powder samples was from 3 to 70° 2θ with a speed of 1° 2θ min^{-1}, operating in the continuous acquisition mode with a current of 20 mA, and CuKα radiation with a monochromator of graphite crystals attached, operating at a tension of 40 kV.

The diffractograms were interpreted based on the relationship of the diffraction peaks for the interplanar spacings (d) present in the structures of the minerals and on the behavior of the diffraction peaks in response to the thermal and $MgCl_2$ and KCl saturation treatments, as described by Moore and Reynolds (1997). Halloysite and kaolinite were differentiated according to the method proposed by Churchman et al. (1984), in which the oriented samples of the clay fraction were subjected to pulverization with formamide and then analyzed through X-ray diffraction.

Due to the impossibility of detection of minerals at concentrations lower than 3 % by the X-ray diffractometer used, the mineral composition of the coarse sand and fine sand fractions of the main horizons of P1, P3, and P4 was determined according to macroscopic properties, e.g., color, brightness, and cleavage, with the aid of a binocular stereoscopic microscope with 160x magnification and incident and transmitted illumination, as proposed by Leinz and Campos (1979).

Thermogravimetric analysis (TGA) of the iron-free clay samples (Mehra and Jackson, 1960) was performed using samples saturated with Mg^{2+} (1 mol L^{-1} $MgCl_2$ solution). Twenty milligrams of clay in alumina crucibles were analyzed from 35 to 1100 °C, with a heating rate of 10 °C min^{-1}, in an N_2 gas atmosphere in a DTA-TGA Netzsch STA 449 analyzer. Some horizons of the profiles were not subjected to TGA because all the extracted clay fractions had previously been used in X-ray diffractometry.

Gibbsite and kaolinite were quantified based on the mass loss evidenced by the TGA, with intervals measured by the thermal events generated by differential thermal analysis (DTA). The data obtained were processed using the software Proteus® 5.1, Netzsch.

The TGA analysis was used only to quantify gibbsite and kaolinite. The amount of gibbsite was determined using the mass loss of the sample between 250 and 350 °C, in comparison to a calculated mass loss corresponding to complete dehydroxylation of a pure gibbsite sample. Kaolinite quantification was calculated analogously, according to the method described in Karathanasis (2008).

The concentration of more crystalline iron oxides (goethite - Gt - and hematite - Hm) was also determined in samples of the clay fraction concentrated by the removal of kaolinite and gibbsite through boiling with 5 mol L^{-1} NaOH once, 0.5 mol L^{-1} HCl once, $(NH_4)_2CO_3$ twice, and distilled water twice (Norrish and Taylor, 1961; Kämpf and Schwertmann, 1982). The samples were analyzed as non-oriented powder through X-ray diffractometry in the range from 10 to 70° 2θ and speed of 1.0° 2θ min^{-1}, operating in the continuous acquisition mode.

After impregnation of the undisturbed samples from horizons Bi2 of P1, BC3 of P2, Bt1 and Bt3 of P3, and Bt of P4 contained in Kubiena boxes, micromorphological thin sections were produced using a standard petrography thin sectioning machine. The blocks were glued onto glass slides using Araldite® glue. Polishing was performed using the abrasive layer of silicon carbide on a rotary disc machine. The final touch was performed manually with abrasive powder until the quartz crystals reached the desired extinction pattern in an optical microscope.

Micromorphological description was performed under natural and polarized light in a petrographic microscope (Olympus BX51) attached to a digital camera (Olympus SC20). The micromorphological descriptions were conducted according to Bullock et al. (1985).

RESULTS AND DISCUSSION

Soil classification, and macromorphological and physical properties

According to the criteria established by the SiBCS (Santos et al., 2013), World Reference Base of Soil Resources (WRB, 2014) and Soil taxonomy (Soil Survey Staff, 2014), the distribution of the soil classes from the top to the lower third of the toposequence is in the following order: P1 - *Cambissolo Háplico Tb Distrófico típico*, Haplic Cambisol, or Dystric Haplustept (Figure 2a); P2 - *Argissolo Vermelho-Amarelo Distrófico abrúptico*, Abruptic Lixisol, or Inceptic Hapludult (Figure 2b); P3 - *Argissolo Vermelho-Amarelo Distrófico típico*, Haplic Lixisol, or Inceptic Hapludult (Figure 2c); and P4 - *Argissolo Vermelho-Amarelo Distrófico típico*, Haplic Lixisol, or Typic Hapludult (Figure 2d).

The profiles are differentiated in horizons in the sequence: A-AB-BA-Bi1-Bi2-C/Cr (P1), Ap-Bt1-Bt2-BC1-BC2-BC3 (P2), Ap-Bt1-Bt2-Bt3-C (P3), and Ap-BA-Bt-Bt/Cr-Cr/C (P4) (Table 1). The sequence of the soils evidences a lower degree of pedogenetic evolution on the top of the slope, leading to the absence of the Bt horizon in this profile (Table 1). The color of the

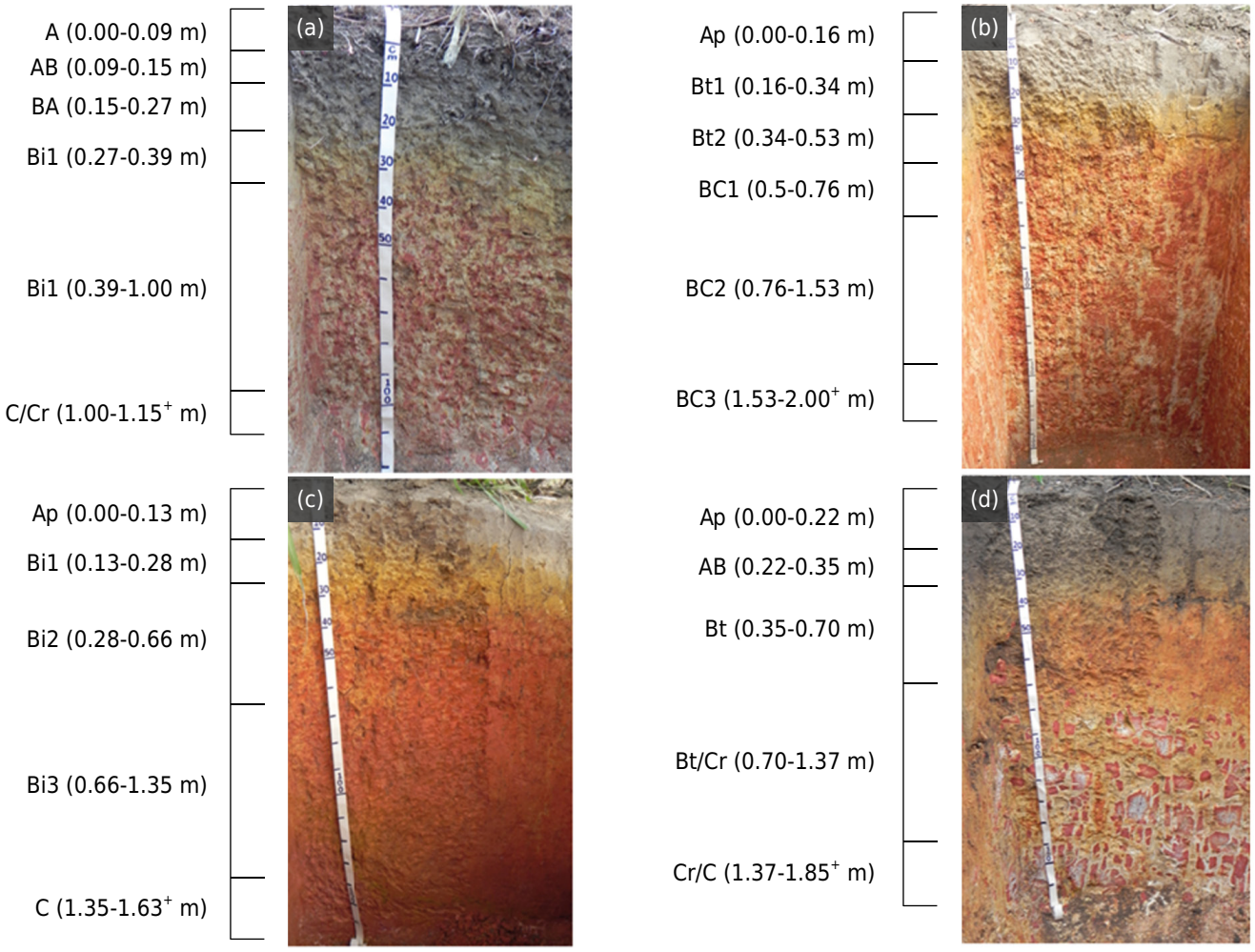

Figure 2. Image of the profiles. (a) Profile 1: *Cambissolo Háplico Tb Distrófico típico* (SiBCS), Haplic Cambisol (WRB), or Haplustept (Soil Taxonomy); (b) Profile 2: *Argissolo Vermelho-Amarelo Distrófico abrúptico* (SiBCS), Abruptic Lixisol (WRB), or Hapludult (Soil Taxonomy); (c) Profile 3: *Argissolo Vermelho-Amarelo Distrófico típico* (SiBCS), Haplic Lixisol (WRB), or Hapludult (Soil Taxonomy); and (d) Profile 4: *Argissolo Vermelho-Amarelo Distrófico típico* (SiBCS), Haplic Lixisol (WRB), or Hapludult (Soil Taxonomy).

matrix of the soils varies from yellowish to reddish (Table 1). There are also mottles in the subsurface of P1 (Figure 2a), P2 (Figure 2b), and P3 (Figure 2d). The surface horizons are grayish-brown (Table 1) due to the higher concentration of organic matter. The saprolite is approximately 1.00, 1.35, and 0.70 m deep in P1, P3, and P4, respectively, while in P2, the weathered rock is below 2.00 m (Table 1); such difference in *solum* thickness may be associated with soil losses through erosion.

The structure of the surface horizons is weak and strong granular (Table 1). In the Ap horizon of P3, there are also subangular blocks, possibly associated with exposure of a subsurface horizon due to a steeper slope (half-slope). The subsurface horizons have subangular and angular blocks, favored by the higher clay contents in the subsurface (Table 1).

The texture varied from clay loam to silty loam in surface horizons to very clayey in the subsurface (Table 1). The predominance of the silt and clay fractions (Table 1) demonstrates how the aphanitic texture of the rhyolite, the process of alteration of primary minerals, and the consequent formation of clay minerals contribute to the particle size distribution of the profiles (Swindale and Jackson, 1960; Heckman et al., 2009).

Clay contents ranged from 242 to 638 g kg^{-1} (Table 1). The clay had been removed from the uppermost surface portion (A horizons) and accumulated in Bt horizons, at depths of 0.16-0.53 m in P2, 0.13-1.35 m in P3, and 0.22-1.37 m in P4. The P2 exhibits abrupt textural change (Table 1) and a lower degree of pedogenetic evolution than P3 and P4, evidenced by the absence of clay illuviation features. In contrast, P1 has a lower degree of evolution of the Bi horizon, without a sufficient B/A textural ratio to be classified as Bt (Table 1).

The aphanitic texture of the rhyolite influenced the high values of the silt/clay ratio (Table 1). This demonstrates restrictions regarding the use of this ratio for rhyolite-derived soils. The clay DF increases in the surface (Table 1), influenced by the higher contents of organic matter (Table 2). The Sd values ranged from 1.16 to 1.53 Mg m^{-3} (Table 1). The use of the soil resulted in compaction of its surface layer, which was reflected in higher Sd values and reduction in total porosity in P2, P3, and P4, compared with P1. The Pd reflected the quartzose mineralogical composition of the silt and sand fractions (Table 1).

Soil chemical properties

The soils are dystrophic and with electronegative features; pH in water ranged from 4.1 to 4.6 (Table 2). The CEC values reduced from 17.1 to 7.1 $cmol_c$ kg^{-1} toward the saprolite, following the variation in TOC, which was also higher in the surface layer (Table 2). This acidity and low CEC reflect the felsic composition of the rhyolite, poor in bases, and the nature of the minerals of the clay fraction.

The losses of Ca^{2+}, Mg^{2+}, and K^{+} through leaching are greater on the slope, while the values of Al^{3+} are high (>2 $cmol_c$ kg^{-1}) and, associated with m values above 50 % across the entire slope, give an alic character to all the soil profiles (Table 2). This expresses the degree of weathering of the soils and the composition of the original rock (rhyolite).

Similar results have been observed in soils of the Cabo Basin (Costa, 2012; Carvalho et al., 2013; Neves, 2014) and in soils developed from the alteration of rhyolites in other regions (Heckman and Rasmussen, 2011). The values of K and P, slightly higher in the surface layer (Table 2), are related to greater supplies of organic matter and/or the fertilization applied in the area.

The soils contain a higher proportion of SiO_2 and a lower proportion of CaO, MgO, and K_2O (Table 2), which reflects residual enrichment of SiO_2 in the uppermost surface horizons. The low K_2O contents in the profiles are consistent with the presence of traces of muscovite and potassium feldspar observed in the sand fraction (Table 2). Weathering and pedogenesis evolution result in losses of SiO_2, CaO, and P_2O_5 and a relative increase

Table 1. Morphological and physical properties of soils in a rhyolite toposequence in the Ipojuca formation, Sirinhaém, PE, Brazil

Horizon	Layer	Color	Texture[1]	Structure[2]			Particle size distribution[3]			CDW	DF	Silt/ Clay	Density		TP
				Grade	Size	Shape	Sand	Silt	Clay				Sd	Pd	
	m						g kg^{-1}				%		Mg m^{-3}		%
P1- Haplic Cambisol (FAO - WRB) / Dystric Haplustept (SSS - Soil Taxonomy)															
A	0.00-0.09	10YR 3/2	Sil Cy Lo	Weak	Sl and Med	Gr	187	571	242	97	60	2.36	1.16	2.50	53
AB	0.09-0.15	10YR 4/3	Sil Cy Lo	Weak and Mod	Sl and Med	Gr and Bl Sub	186	521	293	49	83	1.78	1.23	2.58	52
BA	0.15-0.27	10YR 5/6	Sil Cy Lo	Weak	Sl and Med	Bl Sub	170	488	342	98	71	1.43	1.40	2.62	47
Bi1	0.27-0.39	10YR 6/4	Sil Cy Lo	Weak	Sl and Med	Bl Sub	141	422	437	194	56	0.97	1.46	2.65	45
Bi2	0.39-1.00	10YR 6/8[4]	Cy	Mod	Sl and Med	Bl Sub and Ang	143	377	480	0	100	0.79	1.48	2.67	45
C/Cr	1.00-1.15^{+}	nd	Sil Cy Lo	nd	nd	nd	145	515	340	0	100	1.51	nd	2.67	nd
P2 - Abruptic Lixisol (FAO - WRB) / Inceptic Hapludult (SSS - Soil Taxonomy)															
Ap	0.00-0.16	10YR 4/2	Cy Lo	Weak Ma	Sl	Gr	260	398	342	147	57	1.16	1.53	2.61	41
Bt1	0.16-0.34	10YR 6/8	Cy	Weak Ma	Sl and Med	Bl Sub	136	287	577	0	100	0.50	1.37	2.68	49
Bt2	0.34-0.53	10YR 7/6[5]	Very clayey	Mod	Sl and Med	Bl Sub and Ang	133	244	623	0	100	0.39	1.35	2.70	50
BC1	0.53-0.76	10YR 7/6[6]	Cy	Mod	Sl and Med	Bl Sub and Ang	120	304	576	0	100	0.53	1.38	2.70	49
BC2	0.76-1.53	10YR 7/6[7]	Cy	Mod	Sl and Med	Bl Sub and Ang	109	364	527	0	100	0.69	1.51	2.67	43
BC3	1.53-2.00^{+}	10YR 7/6[8]	Sil Cy	nd	nd	nd	94	428	479	0	100	0.89	1.49	2.70	45
P3 - Haplic Lixisol (FAO - WRB) / Inceptic Hapludult (SSS - Soil Taxonomy)															
Ap	0.00-0.13	10YR 3/2	Sil Cy	Weak and Mod	Sl and Med	Gr and Bl Sub	238	419	343	147	57	1.22	1.41	2.58	45
Bt1	0.13-0.28	10YR 6/8	Cy	Weak	Sl and Med	Bl Sub	126	341	534	49	91	0.64	1.42	2.61	46
Bt2	0.28-0.66	10YR 6/6[9]	Very clayey	Weak and Mod	Sl and Med	Bl Sub and Ang	87	291	622	48	92	0.47	1.42	2.62	46
Bt3	0.66-1.35	10YR 6/6[10]	Cy	Mod	Sl and Med	Bl Sub and Ang	107	315	578	48	92	0.54	1.47	2.67	45
C	1.35-1.63^{+}	nd	Cy	nd	nd	nd	122	348	529	48	91	0.66	nd	2.68	nd
P4 - Haplic Lixisol (FAO - WRB) / Typic Hapludult (SSS - Soil Taxonomy)															
Ap	0.00-0.22	10YR 3/1	Sil Cy Lo	Weak and Ma	Sl and Med	Gr	170	496	334	191	43	1.49	1.41	2.65	47
BA	0.22-0.35	10YR 5/4[11]	Sil Cy	Weak and Ma	Sl and Med	Bl Sub	139	432	429	143	67	1.01	1.44	2.68	46
Bt	0.35-0.70	2,5YR 4/8	Very clayey	Weak	Sl and Med	Bl Sub	63	298	638	46	93	0.47	1.30	2.76	53
Bt/Cr	0.70-1.37	nd	Cy	nd	nd	nd	76	342	582	45	92	0.59	nd	2.68	nd
Cr/C	1.37-1.65^{+}	nd	Sil Cy Lo	nd	nd	nd	145	543	312	45	86	1.74	nd	2.65	nd

[1] Lo: loam; Cy: clay; Sil: silt. [2] Mod: moderate; Sl: small; Med: medium; Gr: granular; Bl: blocky; Ang: angular; Sub: subangular; Ma: massive; nd: not determined. [3] Sand, silt, clay: method described in Gee and Or (2002). CDW: clay dispersed in water (Gee and Or, 2002). DF: degree of flocculation of clay. Sd: soil bulk density (Blake and Hartge, 1986). Pd: particle density (Flint and Flint, 2002). TP: total porosity. [4] Soil mottling (2.5YR 4/8); [5] soil mottling (2.5YR 3/6); [6] soil mottling (2.5YR 3/6, 10YR 7/2); [7] soil mottling (2.5YR 3/6, 10YR 7/2, 7.5YR 5/8); [8] soil mottling (2.5YR 3/6, 7.5YR 5/8, 10YR 5/8); [9] soil mottling (2.5YR 6/6); [10] soil mottling (2.5YR 4/6); and [11] soil mottling (10YR 3/2).

Table 2. Chemical properties of soils in a rhyolite toposequence in the Ipojuca formation, Sirinhaém, PE, Brazil

Hor[(1)]	pH		ΔpH	Ca^{2+}	Mg^{2+}	K^+	Na^+	SB	Al^{3+}	H+Al	CEC	V	m	P	TOC	T	SiO_2	Al_2O_3	Fe_2O_3	TiO_2	CaO	MgO	K_2O	P_2O_5
	H_2O	KCl																						
				cmol$_c$ kg^{-1}								%		mg kg^{-1}	g kg^{-1}	cmol$_c$ kg^{-1}	%							
P1- Haplic Cambisol (FAO - WRB) / Dystric Haplustept (SSS - Soil Taxonomy)																								
A	4.1	3.4	-0.7	2.77	0.52	0.17	0.18	3.7	2.7	13.4	17.1	21.4	42.4	7.29	32.0	70.4	75.8	13.7	2.3	0.4	0.1	nd	0.1	0.1
AB	4.3	3.7	-0.7	2.64	0.30	0.11	0.13	3.2	2.0	10.0	13.2	24.2	38.7	4.93	24.2	44.9	75.0	13.6	3.7	0.4	0.1	0.1	0.1	0.1
BA	4.3	3.7	-0.6	1.39	0.34	0.08	0.10	1.9	2.4	7.9	9.8	19.6	56.3	1.24	12.7	28.8	73.6	15.3	4.0	0.4	nd	nd	0.1	nd
Bi1	4.6	3.8	-0.8	1.34	0.40	0.04	0.14	1.9	2.6	5.4	7.3	26.4	57.9	0.63	7.5	16.8	66.8	20.0	7.1	0.4	nd	nd	0.1	nd
Bi2	4.6	3.8	-0.8	1.51	0.48	0.02	0.11	2.1	3.7	6.2	8.3	25.6	64.1	0.53	3.6	17.3	54.4	27.1	11.2	0.4	nd	nd	nd	nd
C/Cr	4.6	3.7	-0.8	0.98	0.22	0.01	0.17	1.4	4.6	7.5	8.9	15.7	77.2	0.71	2.4	26.0	59.7	25.7	8.3	0.4	nd	nd	0.1	nd
P2 - Abruptic Lixisol (FAO - WRB) / Inceptic Hapludult (SSS - Soil Taxonomy)																								
Ap	4.6	3.9	-0.7	1.68	0.27	0.12	0.18	2.3	0.9	7.8	10.1	22.7	29.6	2.09	12.2	29.5	73.1	15.0	3.6	0.4	0.1	nd	0.1	0.1
Bt1	4.4	3.9	-0.6	1.71	0.26	0.04	0.07	2.2	1.9	6.8	9.0	24.3	47.2	0.79	8.4	15.5	57.0	26.8	9.0	0.5	0.1	nd	nd	nd
Bt2	4.3	3.8	-0.5	1.44	0.44	0.01	0.06	2.0	3.2	6.8	8.8	23.1	62.3	0.82	5.0	14.1	53.6	24.5	14.8	0.7	0.1	nd	0.1	0.3
BC1	4.3	3.8	-0.5	1.40	0.21	0.00	0.20	1.9	3.5	6.7	8.7	22.0	65.4	0.70	3.5	15.0	55.3	27.3	9.0	0.5	0.1	nd	nd	nd
BC2	4.3	3.8	-0.5	0.21	0.43	0.00	0.17	0.8	3.4	6.3	7.1	11.9	80.8	0.45	2.5	13.5	57.2	26.8	8.6	0.4	nd	nd	nd	nd
BC3	4.3	3.8	-0.5	0.15	0.41	0.01	0.21	0.8	3.7	6.8	7.6	10.9	82.2	2.09	2.4	15.9	59.6	25.1	8.6	0.4	nd	nd	nd	nd
P3 - Haplic Lixisol (FAO - WRB) / Inceptic Hapludult (SSS - Soil Taxonomy)																								
Ap	4.2	3.8	-0.4	1.15	0.38	0.04	0.06	1.7	1.5	13.0	14.6	11.4	47.2	11.03	15.3	42.7	74.7	15.4	3.5	0.4	0.1	nd	0.1	0.1
Bt1	4.1	3.9	-0.3	1.17	0.28	0.02	0.04	1.6	2.1	11.3	12.9	12.1	58.1	2.50	8.9	24.1	57.2	26.6	8.5	0.4	nd	nd	nd	nd
Bt2	4.1	3.9	-0.3	1.41	0.37	0.03	0.04	1.9	2.6	11.9	13.8	14.0	58.4	1.31	9.1	22.2	54.8	28.6	9.0	0.5	0.1	nd	nd	nd
Bt3	4.3	3.9	-0.4	1.50	0.24	0.02	0.03	1.9	2.8	10.6	12.4	15.0	60.7	0.78	4.8	21.5	55.8	27.8	9.8	0.4	0.1	nd	nd	nd
C	4.3	3.9	-0.4	0.26	0.47	0.00	0.04	0.8	3.8	11.2	12.0	6.7	82.9	0.42	3.5	22.6	73.1	17.4	2.3	0.2	nd	0.1	0.1	0.1
P4 - Haplic Lixisol (FAO - WRB) / Typic Hapludult (SSS - Soil Taxonomy)																								
Ap	4.2	3.7	-0.5	1.33	0.35	0.06	0.05	1.9	2.1	15.1	17.0	11.2	53.6	12.57	17.2	51.0	71.8	17.0	4.2	0.5	0.1	nd	0.1	0.1
BA	4.3	3.8	-0.5	1.29	0.32	0.02	0.03	1.7	1.8	12.3	14.0	12.4	52.4	2.28	11.8	32.7	52.2	30.1	9.7	0.6	0.1	nd	0.1	0.2
Bt	4.4	3.9	-0.5	1.58	0.42	0.01	0.07	2.3	2.5	12.8	15.1	15.2	54.3	1.31	9.7	23.6	54.4	29.1	10.2	0.5	0.1	nd	nd	nd
Bt/Cr	4.5	3.8	-0.7	1.67	0.20	0.01	0.05	2.2	3.3	13.0	15.2	14.3	62.9	0.84	7.0	26.2	68.1	20.3	3.4	0.7	0.1	nd	0.1	0.2
Cr/C	4.3	3.9	-0.4	1.01	0.38	0.01	0.31	1.9	4.0	13.3	15.3	12.7	69.9	0.77	3.4	49.0	74.0	13.9	4.7	0.3	0.1	nd	0.1	0.1

[(1)] Hor: horizon. SB: sum of bases; CEC: cation exchange capacity; V: base saturation; m: Al saturation, all calculated according to the method described in Embrapa (2009); TOC: total organic carbon (Yeomans and Bremner, 1988); T: clay fraction activity, calculated according to the method described in Embrapa (2009); nd: not determined.

in Fe_2O_3 and Al_2O_3 (Buol and Weed, 1991). In contrast, TiO_2 contents increase slightly with the increase in clay in the subsurface horizons (Table 2).

Soil mineralogical evolution and genesis

Quartz, organic fragments, rock fragments, feldspars, magnetic minerals, opaque minerals, and clayey to ferrous aggregates are the main constituents of the sand fraction in all the profiles (Table 3). Quartz constitutes most of the sand fraction, as observed in the Bi2 horizon of P1 (Figures 3a and 3b). Since it is highly resistant to chemical weathering, the quartz exhibited few signs of alteration (Figure 3a). The size of the quartz in the silt fraction is directly inherited from the aphanitic texture (Pedron, 2007). The presence of minerals in the sand fraction of the profiles occurs because the soils are derived from a porphyritic rhyolite, as already described by Lima Filho (1998) in the Cabo Basin region.

The sand fraction of the profiles showed individual minerals, e.g. quartz and agglomerates of primary minerals in the form of rock fragments, as those present in the BC3 horizon of P2 (Figures 3c and 3d). The presence of these fragments evidences the existence of intermediate weathering stages of the structure of the alteration profiles (Le Pera et al., 2011). Trace quantities of moderately altered muscovite are present in the sand fraction of P3 (Table 3). The potassium feldspar, as observed in the BC3 horizon of P2 (Figures 3e and 3f), also showed a moderate degree of alteration.

Table 3. Qualitative and quantitative mineralogical composition of the coarse sand and fine sand, Fe - Extracted by DCB (Fe_d) and OAA (Fe_o), quantification of kaolinite and gibbsite in the clay fraction, and specific surface area of clay minerals of soils in a rhyolite toposequence in the Ipojuca formation, Sirinhaém, PE, Brazil.

Hor[1]	Layer	Coarse sand[2]	Fine sand[3]	Fe_d	Fe_o	Fe_o/Fe_d	Fe_d/Fe_t	K	Gb	SSA
	m			—— g kg^{-1} ——				——— % ———		m^2 g^{-1}
P1 - Haplic Cambisol (FAO - WRB) / Dystric Haplustept (SSS - Soil Taxonomy)										
A	0.00-0.09	Q 94 % O.F. 4 % R.F. 1 % Agr. 1 % M.op. tr	Q 98 % O.F. 1 % F.R+Agr.1 % M.op. tr	0.54	0.43	0.79	0.47	80.5	0.700	8.1
AB	0.09-0.15	nd	nd	0.51	0.47	0.92	0.53	nd	nd	9.5
BA	0.15-0.27	nd	nd	0.71	0.51	0.72	0.49	nd	nd	12.3
Bi1	0.27-0.39	nd	nd	1.26	0.35	0.28	0.64	64.3	0.003	13.1
Bi2	0.39-1.00	Q 1 % R.F. 98 % M.op.+ Agr. 1 %	Q 55 % F.R 44 % M.op.+Agr 1 %	3.22	0.62	0.19	0.88	nd	nd	17.8
C/Cr	1.00-1.15+	Q 1 % R.F. 94 % Agr. 5 % M.op.<1 %	Q 55 % R.F. 44 % M.op.+Agr. 1 %	1.81	0.47	0.26	0.61	64.0	0.003	20.3
P2 - Abruptic Lixisol (FAO - WRB) / Inceptic Hapludult (SSS - Soil Taxonomy)										
Ap	0.00-0.16	nd	nd	0.59	0.34	0.58	0.73	85.0	nd	11.0
Bt1	0.16- 0.34	nd	nd	2.00	0.32	0.16	0.71	nd	nd	12.6
Bt2	0.34-0.53	nd	nd	1.88	0.71	0.38	0.60	83.8	nd	17.3
BC1	0.53-0.76	nd	nd	2.08	0.62	0.30	0.55	nd	nd	15.5
BC2	0.76-1.53	nd	nd	1.95	0.58	0.30	0.76	nd	nd	14.9
BC3	1.53-2.00+	nd	nd	2.24	0.52	0.23	0.80	76.1	nd	16.9
P3 - Haplic Lixisol (FAO -WRB) / Inceptic Hapludult (SSS - Soil Taxonomy)										
Ap	0.00-0.13	Q 98 % O.F. 1 % R.F. 1 % Agr. 1 % M.mag. tr Mu. tr	Q 99 % O.F. 1 % Agr tr	0.72	0.37	0.51	0.79	81.5	nd	12.4
Bt1	0.13-0.28	nd	nd	1.49	0.37	0.25	0.79	nd	nd	13.7
Bt2	0.28-0.66	Q 80 % O.F. 10 % R.F.8 % Agr. 2 % M.mag. tr	Q 99 % O.F.<1% R.F.+Agr.<1 %	2.36	0.57	0.24	0.76	89.2	nd	10.8
Bt3	0.66-1.35	nd	nd	3.48	0.43	0.12	0.72	nd	nd	10.1
C	1.35-1.63+	Q 10 % O.F. 1 % R.F. 4 % Agr.85 % M.mag .<1 %	Q 99 % R.F. tr Agr. 1 % M.op. tr	2.20	0.29	0.13	0.74	62.5	nd	8.8
P4 - Haplic Lixisol (FAO -WRB) / Typic Hapludult (SSS - Soil Taxonomy)										
Ap	0.00-0.22	Q 92 % O.F. 6 % Agr. 1 % M.mag.+M+Fd <1 %	Q 95 % O.F. 5 % Agr. tr Fd tr	0.52	0.40	0.76	0.36	76.2	nd	9.2
BA	0.22-0.35	nd	nd	0.62	0.61	0.98	0.41	nd	nd	8.6
Bt	0.35-0.70	Q 47 % O.F. 50 % R.F.2 % Agr. 1 % M.mag. tr	Q 99 % O.F. 1 % Agr.+R.F.<1 %	2.41	0.51	0.21	0.83	88.9	nd	8.3
Bt/Cr	0.70-1.37	nd	nd	1.63	0.24	0.15	0.78	nd	nd	14.8
Cr/C	1.37-1.65+	Q 100 %	Q 45 % F.R 55 % Agr. 1 %	0.67	0.23	0.33	0.39	60.4	0.006	8.1

[1] Hor: horizon. [2] Coarse sand: particles with a diameter of 1-2 mm. [3] Fine sand: particles with a diameter of 0.05-1.00 mm. SSA: specific surface area (Quirk, 1955); K: kaolinite; Gb: gibbsite; nd: not determined; O.F.: organic fragments; R.F.: rock fragments; Q: quartz; Fd: feldspar; M.mag: magnetic mineral; M.op: opaque minerals; Agr.: clay aggregates; tr: trace; Mu: muscovite.

Ferruginous nodules distributed in the sand fraction of all the profiles are a product of the alteration of ferromagnesian minerals and opaque minerals. These opaque minerals were observed in all the profiles, e.g., the Bt3 horizon of P3 (Figure 3g). Some of these minerals exhibit strong alteration, as those described in the Bt horizon of P4 (Figure 3h).

The nodules present in the profiles were described as aggregate nodules, e.g., the Bt3 horizon of P3 (Figure 4a), and impregnative nodules, e.g., the Bt horizon of P4 (Figure 4b). Aggregate nodules have an internal fabric that is pure, completely impregnated and in dissolution, impregnating the surrounding matrix with various shades of red. In addition, impregnative nodules have two types of internal fabric: in the center, the internal fabric is red, due to the large presence of hematite (Figure 4b) and on the edges,

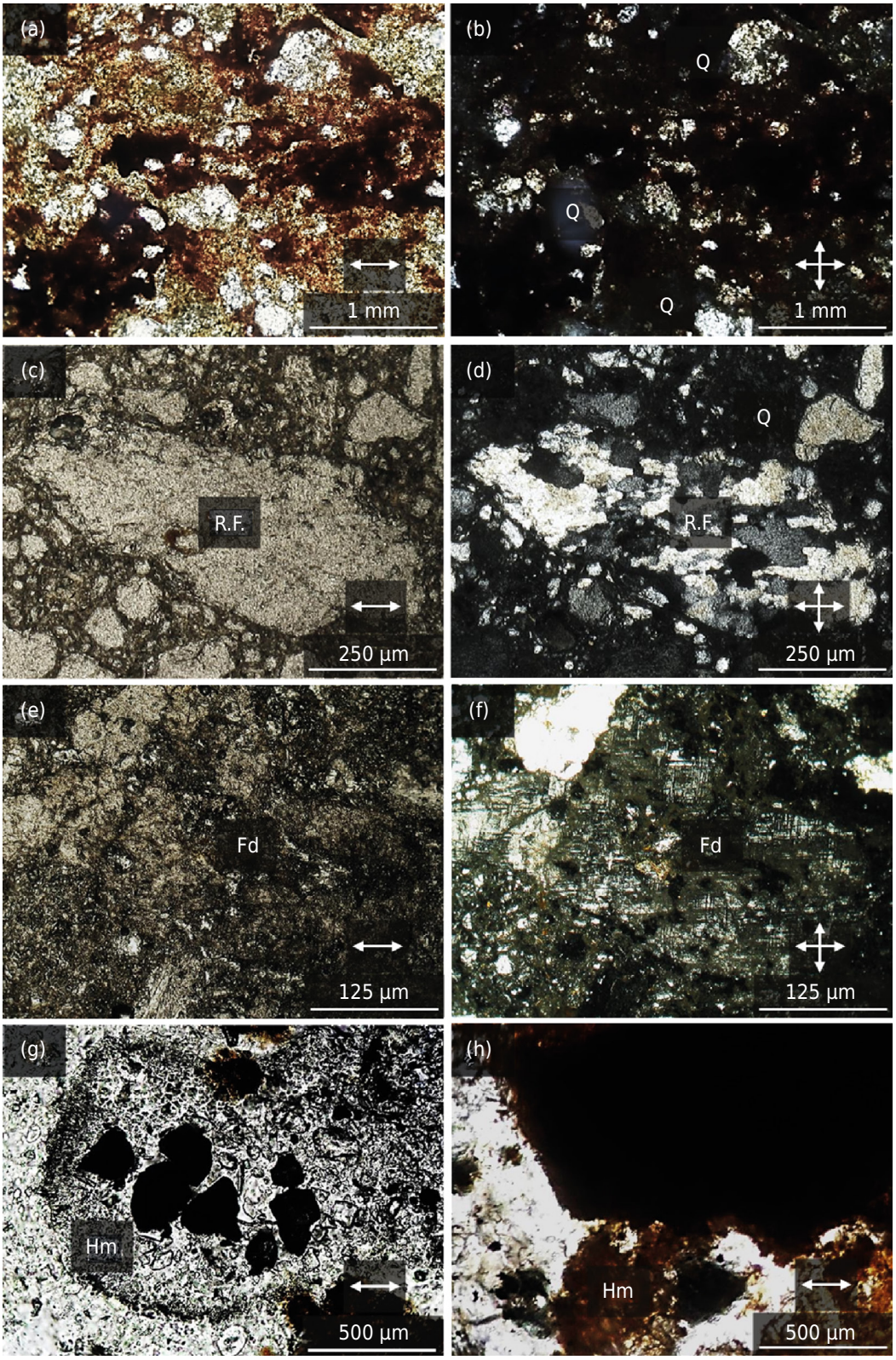

Figure 3. Optical microscopy photographs of alteration features of the quartz, potassium feldspar, and rock fragments in the profiles. (a) Quartz crystals slightly altered in the sand fraction of the Bi2 horizon in P1 (ppl); (b) Quartz crystals slightly altered in the sand fraction (xpl); (c) Fragment of rock formed by quartz in the sand fraction of the BC3 horizon in P2 (ppl); (d) Fragment of rock formed by quartz in the sand fraction (xpl); (e) Potassium feldspar in the sand fraction of the BC3 horizon in P2 (ppl); (f) Potassium feldspar in the sand fraction (xpl); (g) Opaque minerals, probably primary hematite or magnetite, in the Bt3 horizon of P3 (ppl); and (h) Opaque minerals, probably primary hematite or magnetite, with a strong alteration in the Bt horizon in P4 (ppl). Q: quartz; R.F.: rock fragment; Fd: feldspar; Hm: hematite.

the internal fabric has varied shades of brown and yellow, due to the respective presence of diluted hematite and goethite (Figure 4b) (Bullock et al., 1985).

The disintegration of the nodules resulted in the formation of a fine secondary material with color ranging from red to yellow (Figure 4a). Buol and Weed (1991) associated this fine material with the formation of a secondary mineral composition constituted by iron oxides. These structures form approximately 40 % of the ferruginous nodules present in the profiles. The soil matrix close to these nodules is impregnated by a fine material with color ranging from red to yellowish-red (Figure 4b).

The pigmentation of the soil matrix by goethite and hematite is one of the main processes responsible for the development of the yellowish-red color in the profiles studied (Table 1). The pigmentation of the soil matrix from the nodules is corroborated by the fact that the quartz grains are partially coated by reddish brown iron oxide layers close to the ferruginous nodules (Figure 4a). In addition, the variation of color, from red to yellow, suggests the destabilization of the hematite structure and its conversion to goethite through the xanthization process (Oliveira et al., 2004).

A possible altered green hornblende (Figure 4c) could be observed in the BC3 horizon of P2. This possible member of the amphibole group has an alteration morphology close to that described by Cremeens et al. (1992) for this class of mineral. The prismatic morphology of the hornblende leads to the formation of altered structures involved in fine oxidized material, with angular and elongated edges parallel to the x crystallographic axis (Figure 4d). Observing the mineral represented in figure 4c under greater magnification, remnants of the original green color can be noted, in addition to the altered parts with wide formation of fine oxidized material, also along the cleavage planes (Figure 4e).

The fine material observed results from probable deposition and later oxidation of Fe^{2+} in a more soluble form, which starts to form micromorphological features of the quasi-coating and discontinuous infilling types in the inter-aggregate planar pores in contact with the peds. These red and yellowish-red coatings contrast with the whitish color of the soil matrix in the non-impregnated regions, as observed in the BC3 horizon of P2 (Figure 4f).

In the Bt1 horizon of P3, at a depth of 0.30 m, root tissues were also impregnated by this fine material derived from the oxidation of more soluble forms of iron (Figure 4g). This fine oxidized material can be observed impregnating cell walls, intracellular content, and pores, promoting a red color surrounded by a fine yellowish-red material (Figure 4h).

The alterations of the feldspars, from the original rhyolite (Figure 5a) to the soil (Figures 3e and 3f), followed three direct routes: (1) dissolution of the crystal already in the sand fraction (Figures 3c and 3d), evidenced by its absence in the silt fraction (Figure 5b), followed by the neoformation of kaolinite (monosialitization), which starts to constitute the clay fraction (Figures 5c, 5d, and 5e) under the condition of strong desilication, also observed by Le Pera et al. (2001) in gneiss-derived profiles; (2) dissolution of the crystal in the sand fraction, as just described, followed by neoformation of gibbsite (allitization) (Figure 5c), under the condition of total desilication, as reported by Buol and Weed (1991); and (3) under the condition of maintenance of higher soil moisture, monosialitization leads to the formation of halloysite (Figure 5e), as described by Kretzschmar et al. (1997) for biotite.

Following an indirect route, the alteration of plagioclase underwent an intermediate stage with the formation of a feldspar-kaolinite pseudomorph in the silt fraction, as evidenced by the presence of kaolinite in the silt fraction of P3 and P4 (Figure 5b), which was described by Taboada and García (1999).

Mineralogical characterization of the clay fraction

Kaolinite is the main clay mineral present in all the horizons of P1 (Figure 5c), P3 (Figure 5d), and P4 (Figure 5e). Kaolinite was identified through the diffraction peaks at 0.724 nm (d_{001})

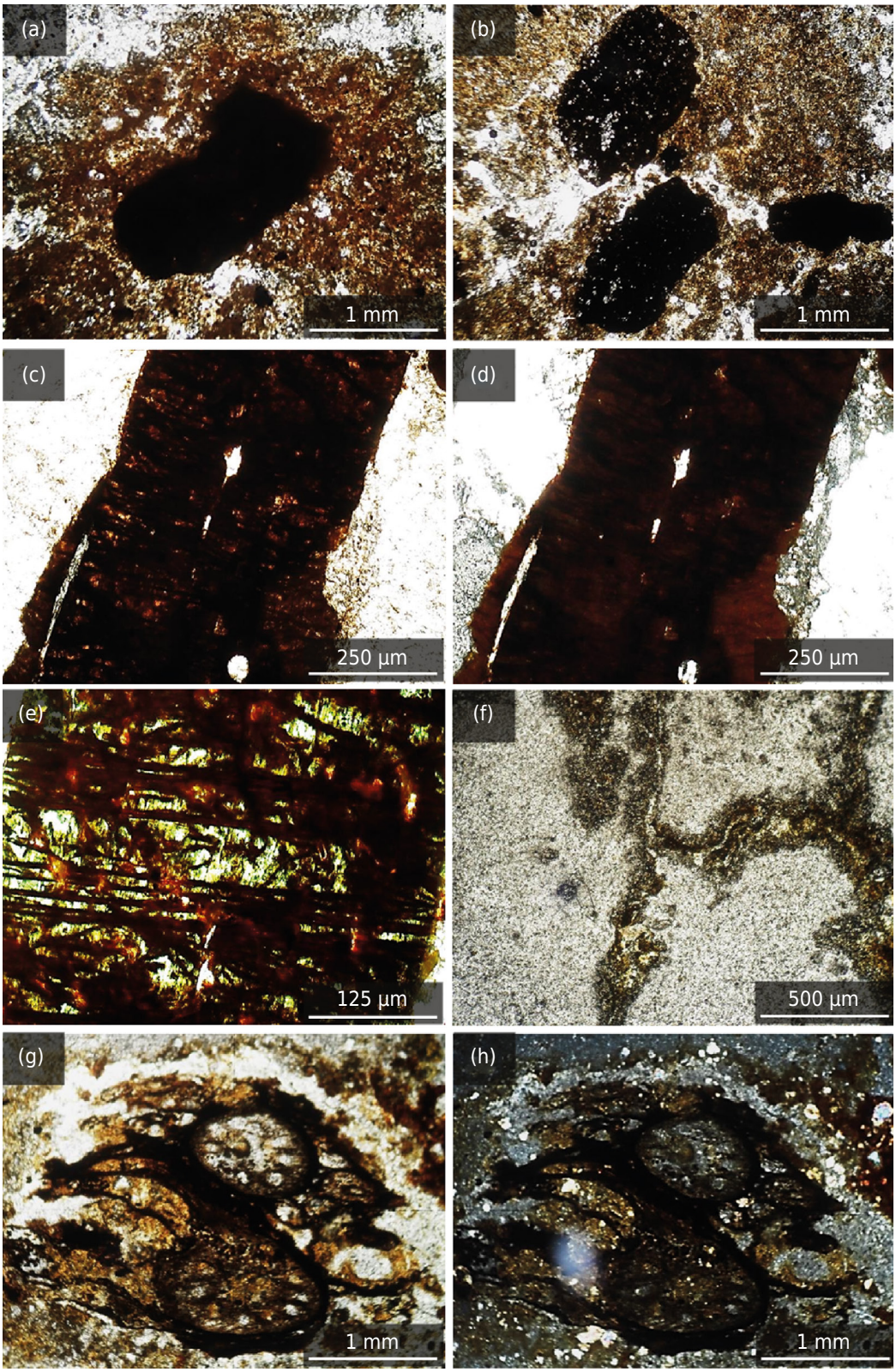

Figure 4. Optical microscopy photographs of the main micromorphological features of the profiles. (a) Nodule aggregates in the Bt3 horizon of P3 (ppl); (b) Impregnative nodules in the Bt horizon of P4 (ppl); (c) Possible altered green hornblende surrounded by oxidized thin material in the BC3 horizon of P2 (ppl); (d) Possible altered green hornblende (xpl); (e) Remnants of color and cleavage of possible green hornblende in the BC3 horizon of P2 (ppl); (f) Coatings and fillings in inter-aggregate planar voids in the BC3 horizon of P2 (ppl); (g) Impregnation of root tissue by fine red and yellow-red materials in the Bt1 horizon of P3 (ppl); and (h) Impregnation of root tissue by fine materials (xpl).

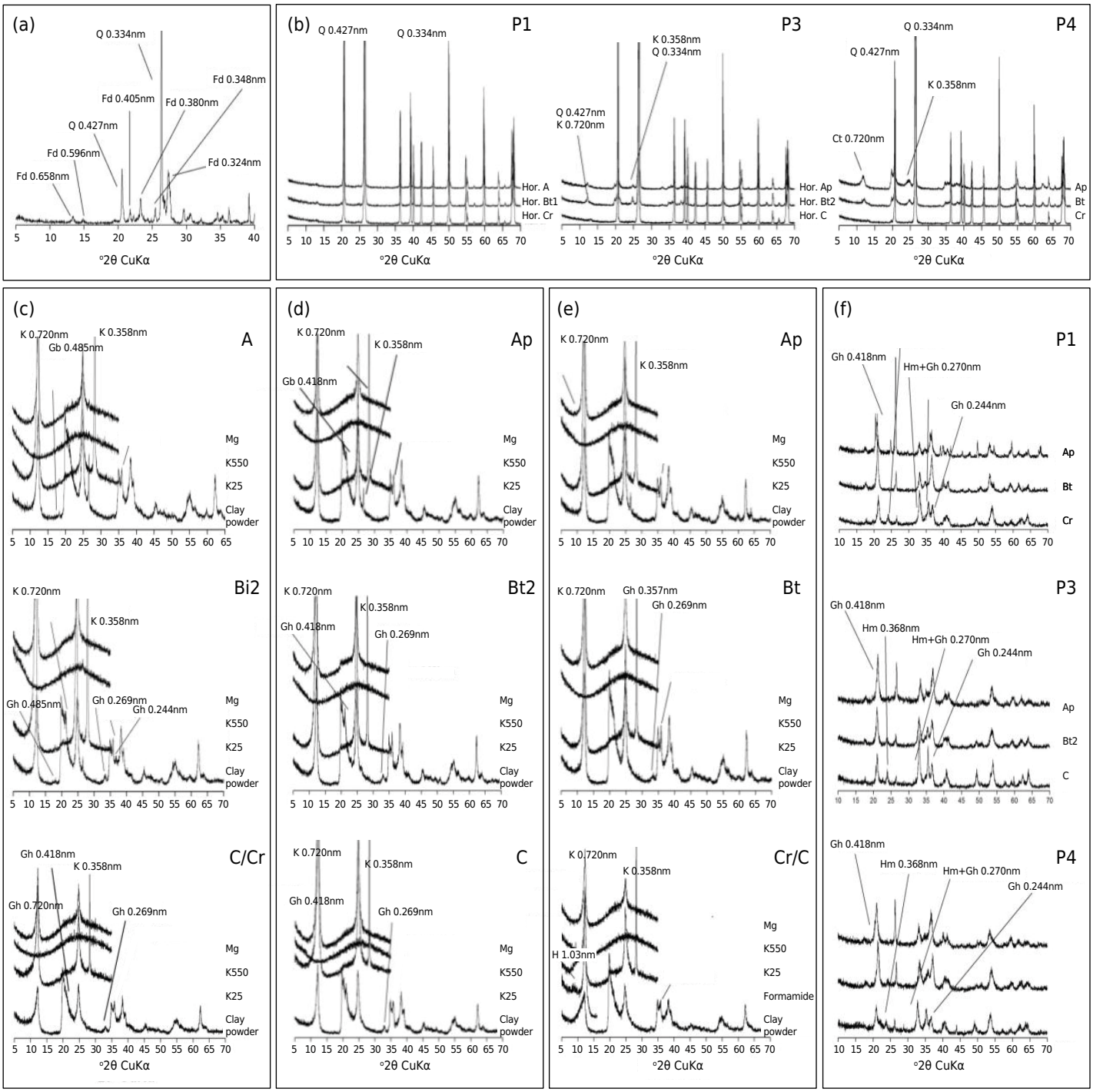

Figure 5. Mineral composition of the samples. (a) X-ray diffraction patterns of the original rock; (b) X-ray diffraction patterns of the silt fraction of the main horizons of P1, P2, and P3; (c) X-ray diffraction patterns of the clay fraction of the main horizons of P1; (d) X-ray diffraction patterns of the clay fraction of the main horizons of P3; (e) X-ray diffraction patterns of the clay fraction of the main horizons of P4; and (f) X-ray diffraction patterns of the oxide concentration of the main horizons of P1, P3, and P4. Q: quartz; Fd: feldspar; K: kaolinite; Gb: gibbsite; Gh: goethite; Hm: hematite; H: halloysite.

and 0.357 nm (d_{002}), which collapsed after heating at 550 °C for 4 h. Gibbsite was detected only in the A and Bi horizons of P1 (Figure 5c) through the peak at 0.485 nm (d_{002}), and goethite was identified through the peak at 0.418 nm (d_{110}).

The presence of kaolinite and gibbsite evidences considerable loss of silica (Buol and Weed, 1991) and the existence of the monosialitization process in P3 and P4, as well as allitization in P1. The presence of these minerals in the clay fraction of the profiles demonstrates the influence of the local climate, hot and humid, for the genesis of soils with degrees of weathering evolution that range from moderate to high (Silva et al., 2013).

Halloysite was also identified (Figure 5e). Halloysite and kaolinite were differentiated according to the method proposed by Churchman et al. (1984), in which the presence of halloysite is confirmed by the expansion of the structure of the phyllosilicate after treatment with formamide, evidenced by the diffraction peak at 1.0 nm (d_{001}), while kaolinite does not have expansion and maintains the peak at 0.7 nm (d_{001}). Its presence in this horizon can be attributed to the maintenance of moisture in the deepest region of this soil.

Studying mineralogical properties of soils of the Serra Geral Formation in the southern region of Brazil, Kämpf and Schwertmann (1995) observed disordered kaolinite associated with halloysite. The presence of halloysite was also identified in saprolites of basalt and rhyolite by Kämpf (1995), who reports the possibility of part of the halloysite arising from the alteration of zeolites. However, in regions of a humid tropical climate, with more expressive dry periods, such as the Northeast of Brazil, halloysite is rare or absent (Kämpf, 1995; Yokoyama and Nakashima, 2005).

Hematite, with a peak at 0.368 nm (d_{110}), and goethite, with a peak at 0.418 nm (d_{110}), were also identified in all the horizons of P1, P3, and P4 (Figure 5f). The presence of hematite may be a product inherited from a possible previous pedogenetic environment, where conditions were favorable to the formation of this mineral. However, this hypothesis needs to be confirmed in future studies. The formation of goethite in these soils would be more recent and would be associated with changes in the pedogenetic environment that made it, for example, more favorable to the maintenance of moisture in the soils (Oliveira et al., 2004).

All profiles showed low Fe_d contents (Table 3), due to the low presence of mafic primary minerals in the rhyolites (Pedron, 2007). The Fe_d/Fe_t ratio had values ranging from 0.60 to 0.88 in the subsurface horizons, confirming the presence of primary forms of Fe, such as primary hematite and magnetite (Table 3). The values of the Fe_o/Fe_d ratio are very high and decrease in the subsurface, indicating instability of the pedogenic oxides of higher crystallinity, especially in the uppermost horizons (Table 3). Schwertmann and Taylor (1989) related the higher contents of low-crystallinity Fe compounds and the higher Fe_o/Fe_d ratio in the surface of the soils to the association of Fe with organic compounds, since organic matter can inhibit the crystallization of iron oxides.

The SSA of the clay fraction in all soils of the toposequence were low, ranging from 8.1 to 20.3 $m^2\ g^{-1}$ (Table 3), which may be associated with the good formation of kaolinite, with development of structures also detected in the silt fraction (Figure 5b). The mean contents of 75 % of kaolinite quantified through DTA/TGA show the prevalence of this 1:1 phyllosilicate in the clay fraction (Table 3). The increase in kaolinite in the surface horizons of the profiles (Table 3) is related to higher weathering intensity on the surface of the regoliths (Buol and Weed, 1991; Le Pera et al., 2011). The SSA values found by Heckman and Rasmussen (2011) for rhyolite-derived soils under similar climatic conditions and mineralogical alteration levels were also low, with mean variation from 10 to 15 $m^2\ g^{-1}$.

CONCLUSIONS

The most active pedogenetic processes in the formation of rhyolite-derived soils in the Cabo Basin were monosialitization, ferralitization, and xanthization.

Halloysite is a constituent of the clay fraction only of the profile located at the lowest portion of the landscape.

The acid composition and aphanitic texture of the rhyolite result in soils with a predominance of fine fractions and low sum of bases.

The color of the soils is associated with the alteration of mafic minerals and primary oxides, the formation of ferruginous nodules, gradual conversion of hematite to goethite, and impregnation of the whitish soil matrix by a red and yellowish-red fine material.

ACKNOWLEDGMENT

To the National Council for Scientific and Technological Development (CNPq) for financial support through the Public Notice - MCTI/CNPq No 14/2013 (Proc. No. 486.419/2013-4).

REFERENCES

Assis WF, Berg EAT, Stefani R. Desenvolvimento de esmaltes com formulações a base de riolito. Ceram Ind. 2002;7:42-5.

Blake GR, Hartge KH. Bulk density. In: Klute A, editor. Methods of soil analysis. Physical and mineralogical methods. Madison: American Society of Agronomy; 1986. Pt 1. p.363-75.

Bullock P, Fedoroff N, Jongerius A, Stoops G, Tursina T. Handbook for soil thin section description. 2nd ed. Wolverhampton: Waine Research Publication; 1985.

Buol SW, Weed SB. Saprolite-soil transformations in the Piedmont and Mountains of North Carolina. Geoderma. 1991;51:15-28. https://doi.org/10.1016/0016-7061(91)90064-Z

Carvalho VS, Ribeiro MR, Souza Júnior VS, Brilhante SA. Caracterização de Espodossolos dos Estados da Paraíba e do Pernambuco, Nordeste do Brasil. Rev Bras Cienc Solo. 2013;37:1454-63. https://doi.org/10.1590/S0100-06832013000600003

Churchman GJ, Whitton JS, Claridge GGC, Theng BKG. Intercalation method using formamide for differentiating halloysite from kaolinite. Clays Clay Miner. 1984;32:241-8.

Costa EUC. Caracterização e gênese de Argissolos e Nitossolos na Bacia Cabo, Pernambuco [dissertação]. Recife: Universidade Federal Rural de Pernambuco; 2012.

Cremeens DL, Darmody RG, Norton LD. Etch-pit size and shape distribution on orthoclase and pyriboles in a loess catena. Geochim Cosmochim Acta. 1992;56:3423-34. https://doi.org/10.1016/0016-7037(92)90389-Z

Empresa Brasileira de Pesquisa Agropecuária - Embrapa. Manual de análises químicas de solos, plantas e fertilizantes. 2a ed rev amp. Brasília: Embrapa Informação Tecnológica; 2009.

Flint AL, Flint LE. Particle density. In: Dane JH, Topp GC, editors. Methods of soil analysis. Madison: Soil Science Society of America; 2002. p.229-40.

Gee GW, Or D. Particle-size analysis. In: Dane JH, Topp GC, editors. Methods of soil analysis. Physical methods. Madison: Soil Science Society of America; 2002. p.255-93.

Ghani NLB. Caracterização morfológica, física, química, mineralógica, gênese e classificação de solos altimontanos derivados de riólito e migmatito da Serra do mar - PR [dissertação]. Curitiba: Universidade Federal do Paraná; 1996.

Ghidin AA, Melo VF, Lima VC, Lima JMJC. Topossequências de Latossolos originados de rochas basálticas no Paraná. I - Mineralogia da fração argila. Rev Bras Cienc Solo. 2006;30:293-306. https://doi.org/10.1590/S0100-06832006000200010

Heckman K, Rasmussen C. Lithologic controls on regolith weathering and mass flux in forested ecosystems of the southwestern USA. Geoderma. 2011;164:99-111. https://doi.org/10.1016/j.geoderma.2011.05.003

Heckman K, Welty-Bernand A, Rasmussen C, Schwartz E. Geologic controls of soil carbon cycling and microbial dynamics in temperate conifer forests. Chem Geol. 2009;267:12-23. https://doi.org/10.1016/j.chemgeo.2009.01.004

Kämpf N. Haloisitas em saprolitos de rochas vulcânicas do Rio Grande do Sul. Rev Bras Cienc Solo. 1995;19:179-84.

Kämpf N, Schwertmann U. The 5-M-NaOH concentration treatment for iron oxides in soils. Clay Clay Miner. 1982;30:401-8.

Kämpf N, Schwertmann U. Goethitas na interface solo-rocha em amostras do Rio Grande do Sul e Minas Gerais. Rev Bras Cienc Solo. 1995;19:359-66.

Karathanasis T. Thermal analysis of soil minerals. In: Ulery AL, Drees LR, editors. Methods of soil analysis. Mineralogical methods. Madison: Soil Sci Soc Am; 2008. Pt 5. p.117-60.

Kretzschmar R, Robarge WP, Amoozegar A, Vepraskas MJ. Biotite alteration to halloysite and kaolinite in soil-saprolite profiles developed from mica schist and granite gneiss. Geoderma. 1997;75:155-70. https://doi.org/10.1016/S0016-7061(96)00089-4

Köppen W. Climatologia. México: Fundo de Cultura Econômica; 1931.

Jackson ML. Soil chemical analysis: advanced course. Wisconsin: Madison libraries, 1969.

Le Pera E, Critelli S, Sorriso-Valvo M. Weathering of gneiss in Calabria, Southern Italy. Catena. 2001;42:1-15. https://doi.org/10.1016/S0341-8162(00)00117-X

Leinz V, Campos JES. Guia para determinação de minerais. 8a ed. São Paulo: Nacional; 1979.

Lima Filho MF. Análise estrutural e estratigráfica da bacia Pernambuco [tese]. São Paulo: Universidade de São Paulo; 1998.

Lima Filho MF, Pedrosa FJA, Medeiros AB, Brito MFI, Nóbrega VA, Araújo RD, Mota JA. Geologia da Bacia Cabo - PE. Geociências. 1996;15:223-42.

Mckeague JA, Day JH. Dithionite and oxalate-extractable Fe and Al as aids in differentiating various classes of soils. Can J Soil Sci. 1966;46:13-22. https://doi.org/10.4141/cjss66-003

Mehra OP, Jackson ML. Iron oxide removal from soils and clays by a dithionite-citrate system buffered with sodium bicarbonate. In: Swineford A, editor. Clays and Clay Minerals. London: Pergamon Press, 1960. p.317-27

Moore DM, Reynolds RC. X-ray diffraction and identification and analysis of clay minerals. 2nd ed. Oxford: Oxford University Press; 1997.

Nascimento MAL, Souza ZS, Lima Filho MF, Sá EFJ, Cruz LR, Frutuoso Júnior LJ, Almeida CB, Antunes AL, Silva FCA, Guedes IMG. Relações estratigráficas da província magmática do Cabo, Bacia de Pernambuco, Nordeste do Brasil. Estudos Geol. 2004;14:3-19.

Nascimento MAL, Souza ZS, Arnosio JM, Vasconcelos PMP. Ignimbrito do Engenho Saco, Ipojuca, PE - Registro de vulcanismo explosivo cretácico na província magmática do Cabo. In: Winge M, Schobbenhaus C, Souza CRG, Fernandes ACS, Queiroz ET, Berbert-Born M, Campos DA, editores. Sítios geológicos e paleontológicos do Brasil. Volume II. Brasília, DF: CPRM; 2009. p.1-13.

Neves LVMW. Caracterização de Nitossolos Háplicos - Argissolo Amarelo em um topolitossequência na Bacia Cabo, Sirinhaém-PE [dissertação]. Recife: Universidade Federal Rural de Pernambuco; 2014.

Norrish T, Taylor RM. The isomorphous replacement of iron by aluminum in soil goethites. J Soil Sci. 1961;12:294-306. https://doi.org/10.1111/j.1365-2389.1961.tb00919.x

Oliveira LB, Ferreira MGVX, Marques FA. Characterization and classification of two soils derived from basic rocks in Pernambuco state coast, northeast Brazil. Sci Agric. 2004;61:615-25. https://doi.org/10.1590/S0103-90162004000600009

Pansu M, Gautheyrou J. Handbook of soil analysis - Mineralogical, organic and inorganic methods. Heidelberg: Springer; 2006.

Pedron FA. Mineralogia, morfologia e classificação de saprolitos e Neossolos derivados de rochas vulcânicas no Rio Grande do Sul [tese]. Santa Maria: Universidade Federal de Santa Maria; 2007.

Quirk JP. Significance of surface areas calculated from water vapor sorption isotherms by use of the B.E.T. equation. Soil Sci. 1955;80:423-30.

Santos HG, Jacomine PKT, Anjos LHC, Oliveira VA, Oliveira JB, Coelho MR, Lumbreras JF, Cunha TJF. Sistema brasileiro de classificação de solos. 3a ed. Rio de Janeiro: Embrapa Solos; 2013.

Santos RD, Lemos RC, Santos HG, Ker JC, Anjos LHC, Shimizu SH. Manual de descrição e coleta de solo no campo. 6a ed. Viçosa, MG: Sociedade Brasileira de Ciência do Solo; 2013.

Schwertmann U, Taylor RM. Iron oxides. In: Dixon JB, Weed SB, editors. Mineral soil environments. 2nd ed. Madison: SSSA Book Series; 1989. p.379-438.

Silva AO, Queluz JTG, Klar AE. Spatial distribution of climatic water balance in different rainfall regimes in the state of Pernambuco. Braz J Appl Technol Agric Sci. 2013;6:7-19. https://doi.org/10.5935/PAeT.V6.N1.01

Soil Survey Staff. Keys to soil taxonomy. 12th ed. Washington, DC: United States Department of Agriculture, Natural Resources Conservation Service; 2014.

Swindale LD, Jackson MLA. Mineralogical study of soil formation in four rhyolite-derived soils from New Zealand. New Zeal J Geol Geophys. 1960;3:141-83. https://doi.org/10.1080/00288306.1960.10423590

Taboada T, García C. Pseudomorphic transformation of plagioclases during the weathering of granitic rocks in Galicia (NW Spain). Catena. 1999;35:291-302. https://doi.org/10.1016/S0341-8162(98)00108-8

World Reference Base for Soil Resources - WRB: A framework for international classification, correlation and communication. Food and Agriculture Organization of the United Nations. Rome: IUSS/ISRIC/FAO; 2014. (World Soil Resources Reports, 106)

Yeomans JC, Bremner JM. A rapid and precise method for routine determination of organic carbon in soil. Commun Soil Sci Plant Anal. 1988;19:1467-76. https://doi.org/10.1080/00103628809368027

Yokoyama T, Nakashima S. Color development of iron oxides during rhyolite weathering over 52,000 years. Chem Geol. 2005;219:309-20. https://doi.org/10.1016/j.chemgeo.2005.03.005